# Application of Digital Image Processing Techniques to Detect Through-Thickness Crack in Hole Expansion Test

Daniel J. Cruz [1,2], Rui L. Amaral [1,2], Abel D. Santos [1,2] and João Manuel R. S. Tavares [1,2,*]

1    Instituto de Ciência e Inovação em Engenharia Mecânica e Engenharia Industrial, Campus da FEUP, R. Dr. Roberto Frias 400, 4200-465 Porto, Portugal; up201405104@edu.fe.up.pt (D.J.C.); ramaral@inegi.up.pt (R.L.A.); abel@fe.up.pt (A.D.S.)
2    Faculdade de Engenharia, Universidade do Porto/s/n, R. Dr. Roberto Frias, 4200-465 Porto, Portugal
*    Correspondence: tavares@fe.up.pt

**Abstract:** Advanced high-strength steels (AHSS) have become increasingly popular in the automotive industry due to their high yield and ultimate tensile strengths, enabling the production of lighter car body structures while meeting safety standards. However, they have some setbacks compared to conventional steels, such as edge cracking through sheet thickness caused by forming components with shear-cut edges. When characterizing the formability of sheet metal materials, the hole expansion test is an industry-standard method used to evaluate the stretch-flangeability of their edges. However, accurately visualizing the first cracking is usually tricky and may be subjective, often leading to inconsistent results and low reproducibility with some impact of the operator on both direct and post-processing measurements. To address these issues, a novel digital image processing method is presented to reduce operator reliance and enhance the accuracy and efficiency of the hole expansion test results. By leveraging advanced image processing algorithms, the proposed approach detects the appearance of the first edge cracks, enabling a more precise determination of the hole expansion ratio (HER). Furthermore, it provides valuable insights into the evolution of the hole diameter, allowing for a comprehensive understanding of the material behavior during the test. The proposed method was evaluated for different materials, and the corresponding HER values were compared with the traditional method.

**Keywords:** edge cracking; hole expansion ratio; adaptive image binarization; circular hough transform; advanced high-strength steels

## 1. Introduction

The challenge posed to the automotive industry to improve energy efficiency and develop low-consumption vehicles has led to a demand for lighter construction components [1,2]. Using new materials to reduce weight is crucial in addressing these issues. Advanced high-strength steels (AHSS) and aluminum alloys have been employed to achieve this goal instead of using conventional steels [3]. AHSS typically exhibits high yield and ultimate tensile strengths, which are critical to ensure passenger safety. However, their processing poses setbacks and challenges. During the manufacturing forming process, the material undergoes severe loadings such as bending and stretching, which can result in edge cracking through the sheet thickness due to its low resistance to sheared edge cracking. The term "stretch-flangeability" refers to the ability of sheet metal materials to resist edge cracking when exposed to edge stretching deformation. This property is typically evaluated through hole punching and expansion tests [4].

The Hole Expansion Test (HET) is a commonly used method to assess the resistance and stretch-flangeability of sheared edges, and it is defined by the ISO 16630 [5] standard. In this test, a metallic sheet with a specified hole size is expanded by a conical punch until a

visible through-thickness crack appears. The hole expansion ratio ($HER(\%)$), is calculated according to:

$$HER(\%) = \frac{D_f - D_i}{D_f}, \tag{1}$$

where $D_f$ (mm) and $D_i$ (mm) represent the diameter of the expanded hole and the initial diameter on the sheared surface of the pre-punched hole, respectively.

The occurrence of cracks is typically assessed manually through visual inspection and experience. However, in some cases, the operator may not recognize the right moment to stop the test, leading to crack propagation and, consequently, increasing the measurement of the final hole diameter [6]. This human subjectivity can lead to errors and significant deviations in experimental results. Moreover, for certain materials, edge cracks may occur at varying times for each trial, which can increase the scatter of the hole expansion ratio [7].

There are several approaches to experimentally determine the crack initiation during the hole expansion test. Dunckelmeyer et al. [8] and Panich et al. [9] related the appearance of a through-thickness crack to a possible drop in the punch force-displacement curve. This method may be insufficient for some materials and test conditions, as multiple micro-cracks may appear simultaneously, requiring additional approaches. Leonhardt et al. [10] employed an automated pneumatic system to detect the crack. The authors concluded that the developed approach exhibits sufficient sensitivity to accurately determine the HER for different process parameters, e.g., cutting clearance and initial hole diameter.

One effective method for monitoring the development of through-thickness cracks is the implementation of digital image correlation (DIC) techniques. This optical measurement technique is widely used in experimental mechanics to analyze the displacement and strain of an object or surface by comparing images acquired before and after deformation [11]. By acquiring a continuous sequence of images during the hole expansion process, this approach enables the precise determination of the exact time when edge cracks appear and simplifies the analysis of their propagation around the hole [12]. Additionally, DIC techniques provide the capability to measure the strain distribution surrounding the hole during the expansion process. Chen et al. [13] employed a DIC technique to measure the strain field around the expanded hole on the upper surface of the specimen, which was important for understanding the deformation behavior and failure mechanisms of the material under analysis. Li et al. [14] later employed an ARAMIS system to observe the deformation of the specimen and investigate the influence of experimental methods, such as burr direction, hole manufacturing method, blank thickness, and punch shape, on the hole expansion ratio. Krempaszky et al. [15] and Wang et al. [16] used a digital camera system equipped with two charge-coupled device (CCD) cameras to measure the hole expansion ratio and generate precise 3D images of the through-thickness crack. Barlo et al. [17] investigated the boundary conditions of the HET by introducing draw beads to the experimental setup. Additionally, they used images acquired by a 3D DIC system to evaluate the hole expansion ratio, thereby reducing the impact of the operator-reliant post-processing. Digital image correlation systems typically require sophisticated and expensive equipment, including high-resolution cameras, specialized lenses, and complex calibration procedures. The need for such equipment and procedures can make setting up and implementing DIC techniques for hole expansion testing time-consuming.

Due to the disadvantages associated with DIC systems, the use of digital image processing (DIP) techniques has emerged as a simpler and viable alternative for the detection of through-thickness cracks during the hole expansion test [18]. These techniques refer to a broad range of methods and algorithms used to modify and extract information from digital images [19,20]. Chiriac et al. [21] used a Digital Recording and Measurement System (DRMS) to accurately determine the HER for different dual-phase steels resulting in a reduction in the variability of the hole expansion results. During the test operation, the system acquires and displays the edge of the punched hole in real time. After the test, the acquired image sequence is replayed, enabling a frame-by-frame analysis of fracture development. This semi-automatic analysis allows for the selection of the specific image frame of the

occurrence of a single through-thickness crack. By measuring the inside diameter of the hole at the selected frame, the authors accurately calculate the final hole expansion ratio. A similar approach was employed by Kim et al. [22]. In their study, the authors used a visual system for monitoring the edge expansion and investigated the effects of pre-machined processes on the hole expansion ratio. In both studies, the through-thickness crack is manually identified and analyzed using a pre-acquired image sequence, which can still introduce an element of human subjectivity and impact the consistency and reliability of the results. To address the challenges associated with the manual identification of through-thickness cracks, Choi et al. [23] developed an algorithm for smart crack inspection based on image processing techniques, mainly binarization and blob detection. This algorithm can automatically detect the presence of a through-thickness crack and calculate the corresponding HER value. Park et al. [24] developed an integrated analysis system that combines computer vision with punch load analysis to improve the accuracy of the measurements. The system includes an automated image processing algorithm, which reduces the risk of human error and enables more precise prediction of the measurements.

Cruz et al. [25] developed an instrumented device to acquire the real-time evolution of the hole dimensions during the test. They also developed a DIP tool, based on the Circular Hough Transform (CHT), to automatically detect and measure the different hole diameters, enabling a more accurate determination of the final hole expansion ratio. This methodology is suitable for sheet materials with thicknesses between 0.5 and 3 mm. The results were more consistent and accurate when compared to the traditional manual measurement method. Besides these developments, the moment to measure the HER value, i.e., the through-thickness crack occurrence, is still chosen manually using a pre-acquired image sequence. This article aims to give continuity to the work presented above by exploring different digital image processing techniques to automatically detect the occurrence of cracks in the hole expansion test, contributing to the improvement of prediction not only of the HER value, but also of the evolution of the expanded hole diameter during the test.

## 2. Experimental Setup

The hole expansion tests were conducted according to the ISO 16630 [5] standard using the universal test machine developed by Duarte et al. [26]. Because of its flexible mechanical system, this hydraulic power equipment is commonly used for studying plastic sheet metal forming behavior, and several tests can be performed with this equipment, including Hole Expansion, Erichsen, Nakajima, and Fukui tests, by simply changing the tool setup [27]. A schematic representation of the HET tool setup is represented in Figure 1.

The instrumented device presented in [25] was used to acquire the real-time evolution of the hole expansion throughout the test. The image acquisition system presented in Figure 1 comprises a digital web camera (Microsoft LifeCam Studio Win USB 1080p) with a maximum image resolution of $2560 \times 2048$ pixels and a maximum frame rate of 30 fps, and an illumination device installed at the center of the top of the system. It consists of a high-brightness LED strip that distributes light evenly on the sheared surface of the hole. A conical punch with a cone angle of $60^{\circ}$ and a diameter of $\phi = 25$ mm was coated with a black PVD layer. This type of coating, as shown in Figure 1, creates a high-contrast region in the acquired image between the inner boundary of the expanded hole and the punch surface, which is critical for the identification of the through-thickness crack and the application of DIP techniques. The implemented image acquisition system is directly synchronized with the universal test machine. Therefore, during each test, an image sequence, i.e., video, is recorded, simultaneously with the displacement and punch force signals. The test stops when the operator sees a macro through-thickness crack. At this point, the test specimen is removed, and the HER value is determined using the acquired image sequence and the proposed digital image processing algorithm.
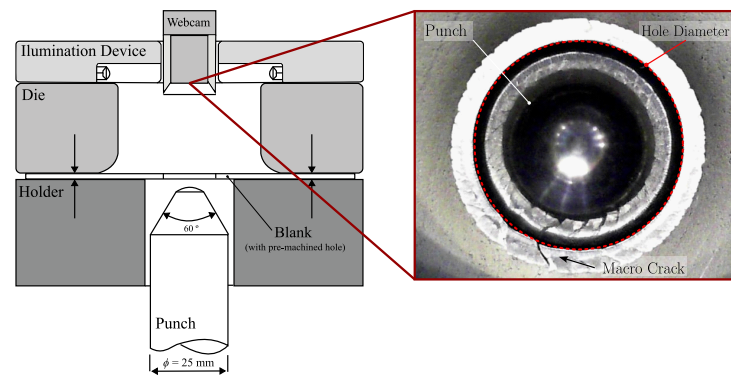
**Figure 1.** Experimental setup used for the hole expansion test (adapted from [25]).

During the hole expansion test, the punch moves vertically, and the plane where the internal diameter is measured approaches the camera successively. As a result, the system resolution, i.e., the ratio between pixels (px) and millimeters (mm), in the measurement plane varies throughout the test. To accurately account for this variability and address any optical distortions, a calibration procedure was performed for different measurement planes using a calibration gauge, depicted schematically in Figure 2. This gauge has marked circles with well-known diameters, $D$, in a range between 6 and 30 mm. The measurement plane is defined as the plane where the inner diameter is measured and its vertical displacement is given by $\Delta d_{m.plane}$. In the presented calibration process, the different measurement plane displacements were defined by approaching the gauge into the camera using the punch movement. The calibration results obtained from this procedure are presented in Figure 2, which lets one perceive the relationship between the known diameters of the gauge circles and their corresponding pixel values.
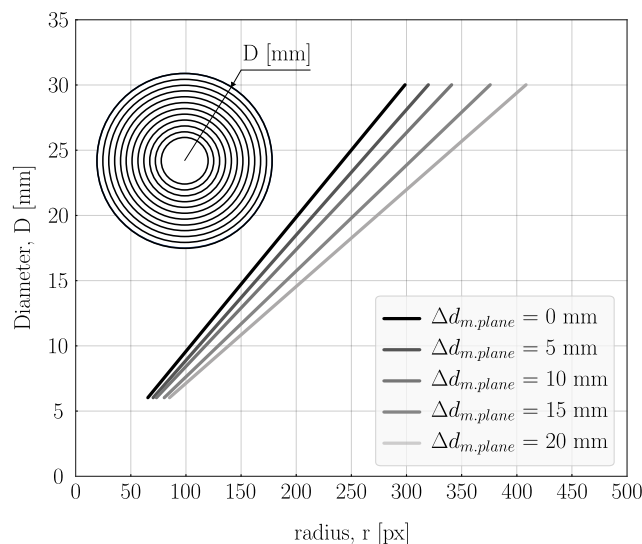


**Figure 2.** Resolution of the used image acquisition system calibrated for different measurement plane displacements, $\Delta d_{m.plane}$ (adapted from [25]).

## 3. Digital Image Processing Algorithm

The first step in the proposed methodology is to automatically extract several images from the pre-recorded image sequence for the experimental test under study. These images are the starting point for applying the digital image processing algorithm, and provide the evolution of the hole size and the through-thickness crack during the test. As shown in Figure 3, the DIP algorithm consists of two distinct steps: (a) crack detection and (b) hole diameter measurement. The crack detection step is responsible for detecting the presence of a through-thickness crack on the sheared surface of the specimen, whereas the hole

diameter measurement step is responsible for measuring the corresponding inner hole diameter of the specimen. If the through-thickness crack is identified, the global algorithm determines the corresponding hole expansion ratio using the initial hole diameter ($D_i$) and the hole diameter determined in the hole diameter measurement step ($D_f$). If no through-thickness crack is detected, the diameter value from the current image is recorded, and the DIP analysis proceeds to the next image for further evaluation. The sub-algorithms corresponding to the crack detection and hole diameter measurement steps are presented in the following sections.
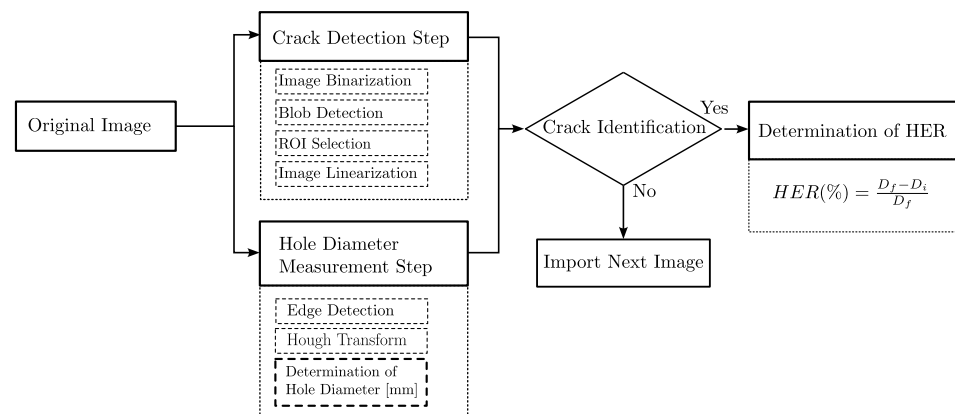


**Figure 3.** Developed digital image processing algorithm for crack identification and hole diameter measurement.

### 3.1. Crack Detection Algorithm

The crack detection step consists of four distinct and successive image processing operations, mainly image binarization, blob detection, selection of the region of interest (ROI), and image linearization. Binarization is the process of creating a binary image from a grayscale image using a thresholding method [28]. All pixel values above a globally determined threshold ($G_t$) are converted to white (a bit value of one), and all other values are set to black (a bit value of zero). Depending on the use of threshold value, the binarization method is divided into global and adaptive binarization. The global binarization method uses a single and constant threshold value for the whole image, whereas the adaptive binarization method uses local threshold values where different threshold values are computed for each pixel in the image. This method offers increased robustness to changes in lighting [29]. The results of both thresholding methods are shown in Figure 4 for an image acquired during the hole expansion test. It is noted that the sheared edge surface is hardly recognized using the global binarization method, as shown in Figure 4b. However, it is possible to obtain a clear binarization image using the adaptive binarization method, as shown in Figure 4c.
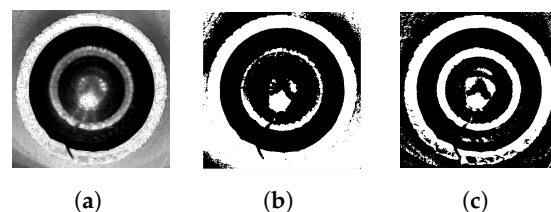


| (a) | (b) | (c) |

**Figure 4.** Binarization methods: (**a**) original image, (**b**) binarized image by global binarization, and (**c**) binarized image by adaptive binarization.

In computer vision, blob detection is a technique used to identify and locate regions or "blobs" in an image that differ in properties, such as brightness, color, or texture, from surrounding regions. These regions or blobs may correspond to objects or features of interest in the input image. For the proposed methodology, different operations were considered,

including (a) the suppression of light structures connected to the image border; (b) the combination of adjacent pixels by filling image regions and holes; and (c) morphological operations, such as closing and boundary extraction [30]. These operations are fundamental for correct and efficient ROI selection. An overview of the blob detection step is shown in Figure 5. After this step, the ROI must be defined for the correct identification of the through-thickness crack. The largest closed area is then selected, resulting in a ring-type structure, as shown in Figure 5d. This structure corresponds to the sheared surface of the pre-punched hole and is the region where the crack identification process is then performed. The parameters used for each operation are summarized in Table 1. These parameters were carefully chosen, taking into consideration the specific characteristics of through-thickness cracks, and were tested to robustly identify macro through-thickness cracks rather than small cracks with a resolution of ±0.1 mm.
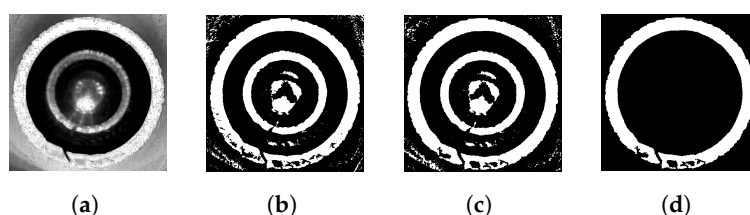


(a)          (b)          (c)          (d)

**Figure 5.** Blob detection and ROI selection steps: (**a**) original image, (**b**) binarized image, (**c**) resultant image after the morphological operations (clear borders and close mask and fill holes), and (**d**) final selected ROI.

**Table 1.** Parameters used in the crack detection algorithm.

| | Method | Adaptive |
|---|---|---|
| **Image Binarization** | Sensitivity | 0.51 |
| | Foreground Polarity | 'bright' |
| | Method | Clear Borders |
| | Pixel connectivity | 8 |
| | Method | Close Mask |
| **Blob detection** | Structuring element | Disk |
| | Size | 1 px |
| | Method | Fill Holes |
| | Pixel connectivity | 4 |
| | Method | Image Filtering |
| **ROI Selection** | Number of returned objects | 1 |
| | Property to filter | Area |
| | Criterium | 'largest' |

The final step of the crack detection algorithm is the so-called image linearization step, which consists of linearizing the sheared edge, as represented in Figure 6, to simplify the through-thickness crack detection. In this step, a new image is built considering a transposition of coordinates for polar coordinates with angles between 0 and 360°. Using this transformation, it is possible to transform the circumferential profile (Figure 6a) of the sheared edge surface into a linear profile (Figure 6b). The center of the desired ROI is determined using the Hough transform [31,32], which is presented in detail in the next section. Analyzing the represented image, it is possible to clearly differentiate the inner and outer boundaries of the shear edge. Furthermore, this type of linear representation is advantageous in identifying whether the through-thickness crack is present. As shown in Figure 6c, the crack is automatically identified when the original image's single ROI blob is divided into two or more independent blobs. In this example, two distinct blobs are marked with different colors (orange and blue), indicating the presence of a crack that extends through the thickness of the material. On the other hand, if the analysis of the linearized image reveals only a single blob within the ROI, it signifies that a crack has not

propagated completely through the material's entire thickness. In such cases, the presence of a single blob suggests that the crack may be localized or partial, rather than extending fully through the material's thickness.
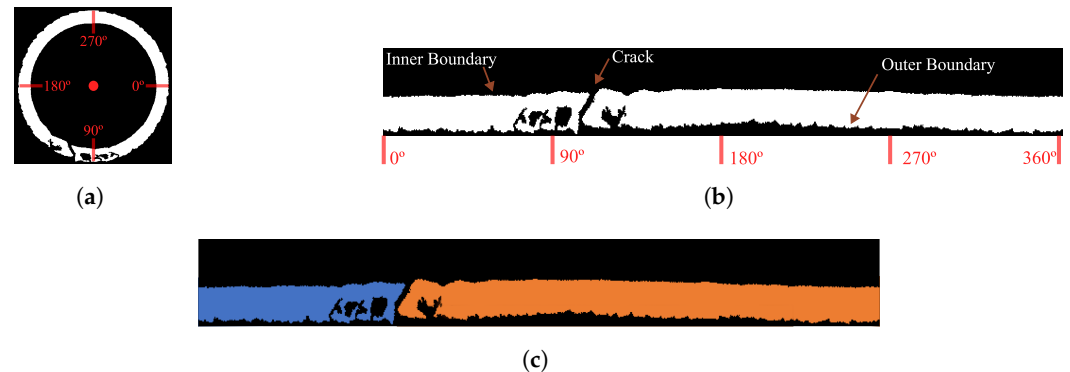


**Figure 6.** Schematic representation of the image linearization procedure: (**a**) original image (ROI), (**b**) linearized image and identification of inner/outer boundaries and through-thickness crack, and (**c**) linearized image and selection of two different blobs.

### 3.2. Hole Diameter Measurement Algorithm

The main objective of the algorithm presented in this section is to identify and measure the hole diameter evolution during the hole expansion test. Figure 7 depicts the different steps of the developed methodology applied to the reference image used in Section 3.1. To detect and measure the diameter value in each image, a Hough Transform (HT)-based algorithm is used. The HT is a popular image processing technique for detecting simple shapes in an image, such as lines, circles, and ellipses. It was first proposed by Paul Hough [33] in 1962 to detect straight lines. Essentially, it works by transforming the image from the original spatial domain to the parameter space, where the shape parameters are represented as points.

The Circular Hough Transform (CHT) is a variation of the HT and is a robust technique used to detect circular shapes, such as circles or arcs, in noisy or distorted images. Duda and Hart introduced it in 1972 [34] as an extension of the original Hough Transform. The CHT transforms the image data from the spatial domain to a parameter space, where circles are represented by their center coordinates $(x, y)$ and radius $(r)$. Each point in the image is represented as a circle in the parameter space, and the accumulation of these circles results in a two-dimensional array called the Hough accumulator, which contains the parameter combinations that receive the most votes. To detect circles using the CHT, the maximum peaks in the Hough accumulator correspond to the center coordinates and radius of the circles in the image. The number of peaks detected corresponds to the number of circles present in the image [35].
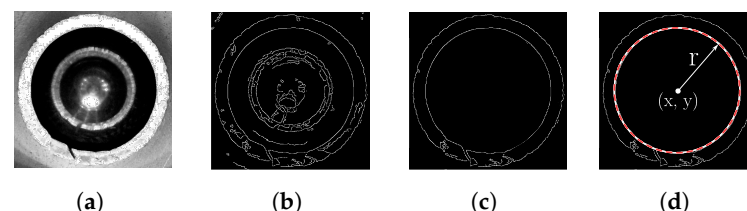


**Figure 7.** Hole diameter measurement algorithm: (**a**) original gray image, (**b**) edge detection using the Canny edge detector, (**c**) selection of the ROI, and (**d**) application of the Circle Hough Transform.

A preliminary edge detection operation must be performed to apply the CHT to an image properly. Edge detection is a digital image processing technique used to identify and highlight an image's edges, defined as the boundaries between two regions with different intensities or color values. The most commonly used edge detection methods are the Sobel operator, the Canny edge detector, and the Laplacian of the Gaussian method. In this work,

the Canny edge detection method [36] is used, which involves multiple steps, such as noise reduction, gradient calculation, non-maximum suppression, and hysteresis thresholding. A threshold value of 0.5 was adopted, resulting in a binary image as the one represented in Figure 7b with a clear and sharp edge highlighted in white [37].

After the edge detection step, several morphological intermediate operations (Figure 7c) are applied to simplify the selection of the region of interest. The CHT is then applied to the selected ROI, as shown in Figure 7d, to obtain each image's inner and outer diameters in pixels. The parameters considered for the edge detection step and Hough Transform are summarized in Table 2. The final inner diameter, $2r$, is converted from pixels to millimeters using a conversion factor that takes into account multiple factors, including the resolution of the acquisition image system, as discussed in Section 2; the thickness of the material; and the displacement of the punch at the time the image was acquired [25]. The methodology described can be applied to sheet materials with thicknesses ranging from 0.5 to 3 mm, and can measure hole diameters with a maximum accuracy of ±0.1 mm.

**Table 2.** Parameters used in the hole diameter measurement algorithm.

| | | |
|---|---|---|
| **Edge Detection Step** | Method | 'Canny Edge' |
| | Threshold Value | 0.5 |
| **Hough Transform** | Method | 'Phase Code' |
| | Edge Threshold | 0.23 |
| | Sensivity | 0.93 |
| | Object Polarity | Bright |

## 4. Application of the DIP Algorithm

The developed DIP algorithm was tested and validated using experimental data from hole expansion tests performed on three distinct ferritic carbon steels [38] with different thicknesses and mechanical properties. Table 3 shows the mechanical tensile properties for each studied material in the rolling direction (RD), according to ISO 6892 [39] and the corresponding thickness value. The holes were produced in each specimen by punching, considering a cutting clearance of 15%. Two samples for each material permit testing results for different materials, thicknesses, and any variability for the current proposed automated procedure. The initial hole diameter, also presented in Table 3, was measured using a Mitutoyo digital three-point internal micrometer with a digital step of 0.001 mm. For each material, the hole expansion test was performed considering a constant punch speed of 0.5 mm/min under a blank holding force of 25 kN. The images were acquired at a rate of 5 fps. In this experimental work, the excessively expanded crack morphology (macro fracture) defined by Li et al. [40] was adopted as the criterion to stop the hole expansion test.

**Table 3.** Tensile properties (RD) and additional information for the studied sheet metal materials.

| Material ID | Thickness t (mm) | Yield Strength Re (MPa) | Ultimate Strength Rm (MPa) | Uniform Elongation A (50%) | Initial Diameter $d_i$ (mm) |
|---|---|---|---|---|---|
| #1 | 2.514 | 480.28 | 548.82 | 26.5 | 10.031 |
| #2 | 2.319 | 517.83 | 581.20 | 23.5 | 10.029 |
| #3 | 1.997 | 577.93 | 611.54 | 24.0 | 10.028 |

*Results*

The force-displacement data obtained for the studied materials during hole expansion are shown in Figure 8. Each curve represents the force–displacement relationship during the hole expansion, with the point of crack identified by the DIP algorithm also indicated. The dotted line on each curve indicates the experimental data acquired between the crack point and the end of the test. The evolution of the punch displacement-force relation exhibits a similar trend for all the studied samples, and the point identified by the DIP

algorithm is consistent across the different materials. Nevertheless, it is important to recognize that the stochastic nature of fracture introduces uncertainty in the observation of the first through-thickness crack and overall fracture behavior.
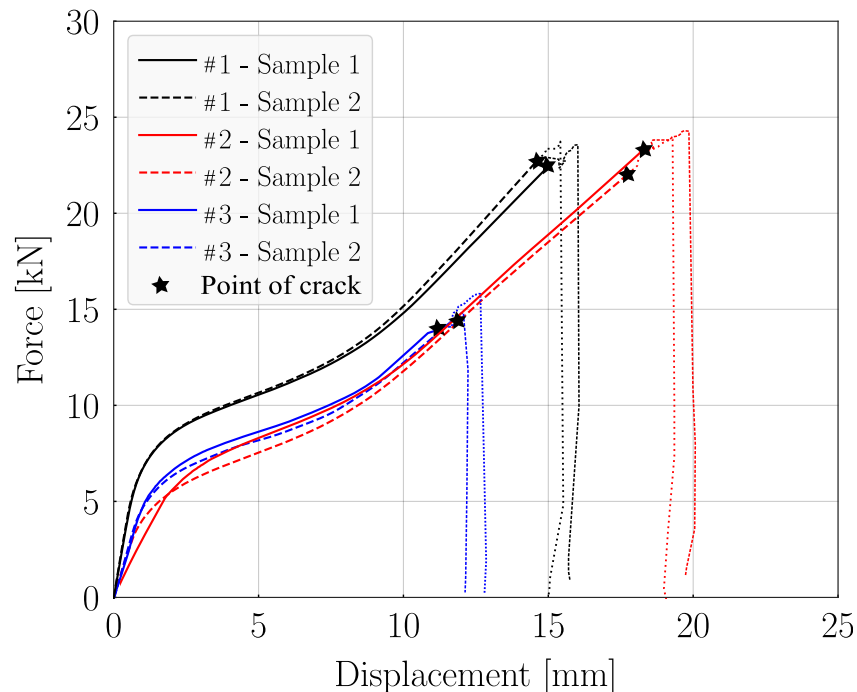


**Figure 8.** HET punch force–displacement curves obtained for the performed hole expansion tests.

As mentioned earlier, the DIP algorithm was developed to detect cracks and measure hole diameters accurately during hole expansion tests. Figures 9–11 show the evolution of the hole diameter during the tests for materials #1, #2, and #3, respectively. Each material has a representative curve of the hole diameter plotted against punch displacement until the point of cracking through the thickness. At this point, the measured diameter corresponds to the final diameter, $D_f$, which is used to calculate the final HER using Equation (1). As can be noted in the analysis of Figure 8, the dotted points beyond the crack point indicate excessive expansion of the hole diameter following crack detection. Unlike the traditional method [39], which evaluates the final diameter after the test has stopped and the punch has been removed, the developed method calculates the HER value using the image acquired when the first macro crack appears. Thus, the HER values obtained using the developed method tend to be lower and more conservative than those obtained by manual measurement, as confirmed by the results presented in Table 4. The table presents the hole-expanded diameter values obtained using the developed DIP algorithm and those measured using a Mitutoyo digital three-point internal micrometer (direct measurement). The corresponding HER values are also presented for each sample. Material #2 has a higher edge crack resistance, presenting a HER value of approximately 73%, in contrast to material #3, which has a lower edge crack resistance (HER $\approx$ 33%). Note that these values are overestimated when direct measurement is used, with HER values of 81.0% for material #2 and 42.5% for material #3. The relative error between samples is below 0.5% for materials #1 and #2, and below 3% for material #3. These values are higher when direct measurement is used, with relative errors of 2.5% for materials #1 and #2, and 6.5% for material #3.

**Table 4.** The HER values obtained by the DIP algorithm and direct measurement.

| Material ID | | | DIP Algorithm | Direct Measurement |
|---|---|---|---|---|
| **#1** | Sample 1 | $D_f$ (mm) | 14.98 | 15.26 |
| | | HER (%) | 49.4 | 52.1 |
| | Sample 2 | $D_f$ (mm) | 15.03 | 15.50 |
| | | HER (%) | 49.8 | 54.5 |
| | Error (%) | HER | 0.4% | 2.4% |
| **#2** | Sample 1 | $D_f$ (mm) | 17.42 | 18.12 |
| | | HER (%) | 73.7 | 80.7 |
| | Sample 2 | $D_f$ (mm) | 17.36 | 18.18 |
| | | HER (%) | 73.2 | 81.3 |
| | Error (%) | HER | 0.5% | 0.6% |
| **#3** | Sample 1 | D (mm) | 13.20 | 14.61 |
| | | HER (%) | 31.6 | 45.6 |
| | Sample 2 | D (mm) | 13.47 | 13.97 |
| | | HER (%) | 34.4 | 39.4 |
| | Error (%) | HER | 2.8% | 6.2% |

Upon analyzing the evolution of the hole diameter with punch displacement in greater detail, it can be realized that the curves for all three materials follow a similar trend. Furthermore, two distinct zones can be identified in the curves. For punch displacements lower than 7.5 mm for materials #1 and #2, and 5 mm for material #3, the hole diameter remains almost constant, with a value equal to the initial diameter ($D_i = 10$ mm), and does not significantly increase with punch displacement. After reaching this point, the evolution of the hole diameter changes significantly, and the relationship between punch displacement and hole diameter becomes linear with a well-defined slope.

At the beginning of the test, the blank is flat, and the inner and outer diameters are coincident. However, as the punch moves, the blank thickness tilts and becomes visible in the acquired image. Therefore, at the start of the test, the DIP algorithm can only detect the outer diameter and begins to detect the inner diameter when the thickness becomes visible in the image. This phenomenon is evident in the results for material #1, where the DIP algorithm only detects and measures the outer hole diameter between 0 (zero) and 5 mm, as it is associated with the tilt of the thickness. In this specific case, an increase in the outer diameter can be observed with punch displacement. After 5 mm displacement, the inner diameter becomes visible in the acquired image and is measured by the proposed algorithm, resulting in a reduction of the estimated value. As the punch advances, the internal diameter is progressively measured, resulting in a linear evolution. A similar analysis can be conducted for the remaining materials.

Figures 9b, 10b, and 11b show, sequentially, the application of the developed DIP algorithm to detect the through-thickness crack and measure the final hole diameter, $D_f$, for materials #1, #2, and #3, respectively. The first image represents the original image, and the second represents the binarized image with the selected ROI. The third represents the linearized image and the identification of the number of blobs. The fourth image shows the result of the edge detection algorithm used to estimate the final hole diameter. The red line in the fifth image represents the estimated diameter. As can be seen, the DIP algorithm was successfully applied to the selected materials, all of which present a single through-thickness crack that generates two independent blobs in the linearized image.
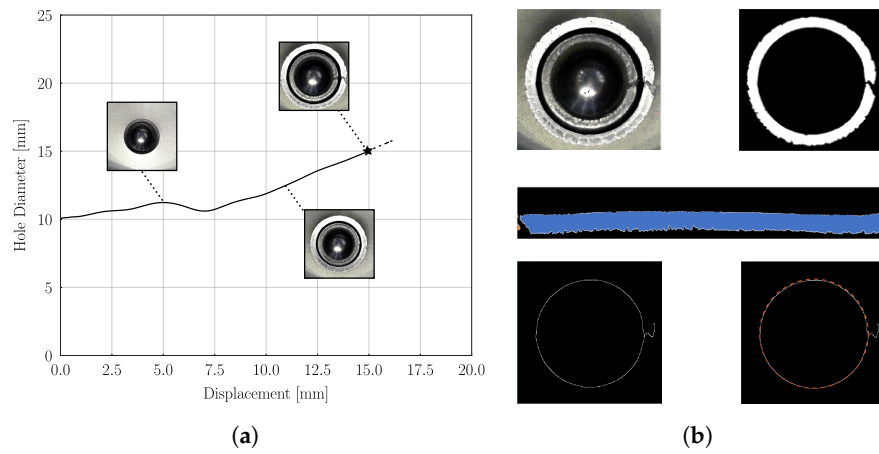
**Figure 9.** Representation of the (**a**) evolution of the hole diameter during the test and the (**b**) application of the developed DIP algorithm to the image with a through-thickness crack for material ID #1.
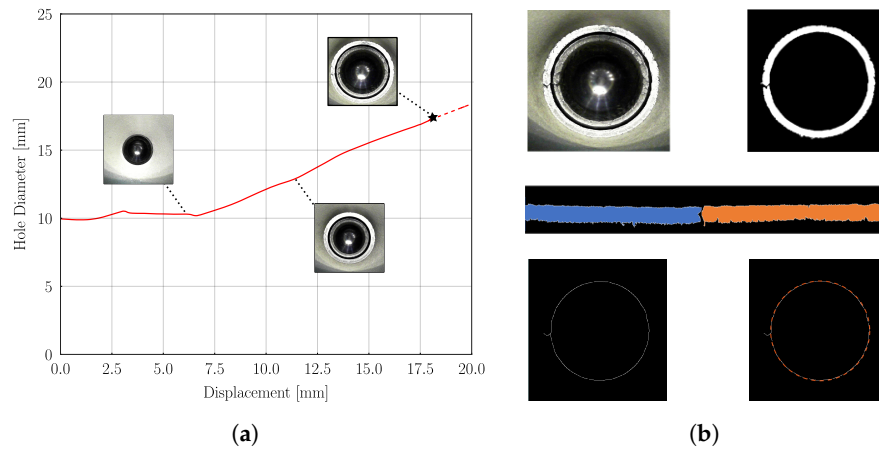


**Figure 10.** Representation of the (**a**) evolution of the hole diameter during the test and the (**b**) application of the developed DIP algorithm to the image with a through-thickness crack for material ID #2.



**Figure 11.** Representation of the (**a**) evolution of the hole diameter during the test and the (**b**) application of the developed DIP algorithm to the image with a through-thickness crack for material ID #3.
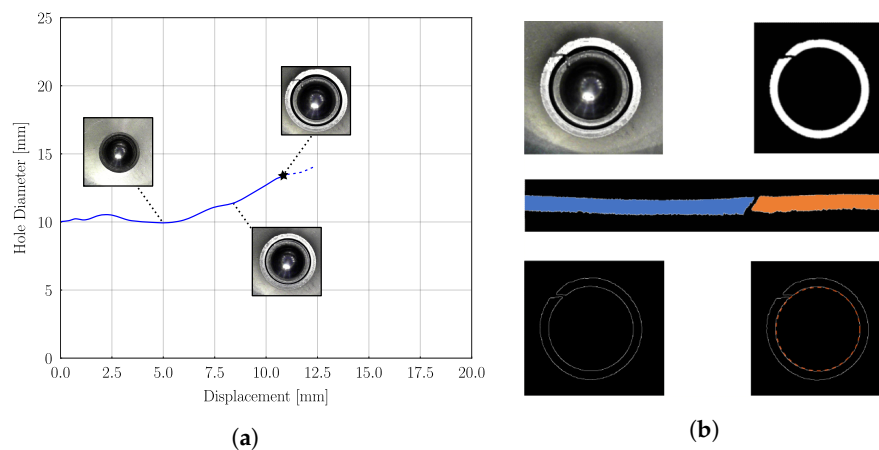
## 5. Conclusions

This work describes a new method based on digital image processing techniques aimed at improving and automating crack detection and final diameter measurement in hole expansion tests. A new experimental image acquisition system was designed to acquire the evolution of the hole during the test, synchronized with the punch displacement and force signals. After the test, a post-processing image processing algorithm is applied to the acquired image sequence to detect the through-thickness crack and measure the different hole diameters.

The developed digital image processing algorithm comprises two sub-procedures: crack detection and hole diameter measurement. The first involves image binarization, blob detection, ROI selection, image linearization, and crack identification. Adaptive binarization is proposed to enhance the versatility of the algorithm, enabling its application to different sheet metal materials and varying thickness values. The algorithm identifies the through-thickness crack when the single ROI blob is separated into several independent blobs in the linearized image. The second uses the Hough transform to identify and measure the inner diameter of the expanded hole during the test. Additionally, the HER value is determined when the through-thickness crack is identified in the crack detection step. The complexity of the developed algorithms is relatively low, as they involve a series of simple operations that do not require high computational costs. Therefore, the simplicity of the operations allows for efficient execution and analysis of the acquired images, making the proposed method practical and accessible for implementation in various experimental settings.

The proposed method was validated using HER tests with three different sheet metals and different thickness values. The results show an excellent accuracy of the automated procedure when compared with manual image sequence analysis of the first thought thickness crack detection. Additionally, the repeatability of the obtained results shows an improvement achieved by the developed methodology due to its superior accuracy. It must be noted that being experimental tests means that material may behave with some uncertainty for fracture and first through-thickness crack observation as a result of the stochastic behavior of fracture. The proposed method with its automated procedure shows a more reliable determination of the Hole Expansion Ratio, being more suited for industrial applications and not dependent on the experience and skills of the test operator.

Future work will focus on experimental validation of the DIP algorithm for materials with different surface treatments, which may have distinct reflectance properties. Furthermore, the algorithm's performance will be assessed in the presence of double cracks, which may exhibit multiple independent blobs. These test conditions may require a more detailed calibration of the algorithm parameters. The effectiveness of the developed algorithm for fully automating the HET test will be evaluated using it during the test rather than just as a post-processing tool. This improvement in the testing methodology will help prevent further crack propagation, as the test will automatically stop once the DIP algorithm detects the presence of a crack, ensuring a more accurate assessment of the hole expansion ratio.

**Author Contributions:** Conceptualization and supervision by A.D.S. and J.M.R.S.T.; data collection, formal analysis, and writing—original draft preparation by D.J.C. and R.L.A.; writing—review and editing by and A.D.S. and J.M.R.S.T. All authors have read and agreed to the published version of the manuscript

**Data Availability Statement:** The data presented in this study are available on request from the corresponding author. The data are not publicly available due to privacy.

**Conflicts of Interest:** The authors declare no conflict of interest.

## Abbreviations

The following abbreviations are used in this manuscript:

| | |
|---|---|
| AHSS | Advanced High-Strength Steels |
| CCD | Charge-Coupled Device |
| CHT | Circular Hough Transform |
| DIC | Digital Image Correlation |
| DIP | Digital Image Processing |
| DRMS | Digital Recording and Measurement System |
| HER | Hole Expansion Ratio |
| HET | Hole Expansion Test |
| HT | Hough Transform |
| PVD | Physical Vapor Deposition |
| ROI | Region of Interest |

## References

1. Hovorun, T.P.; Berladir, K.V.; Pererva, V.I.; Rudenko, S.G.; Martynov, A.I. Modern materials for automotive industry. *J. Eng. Sci.* **2017**, *4*, f8–f18. [CrossRef]
2. Ghosh, A.G.M.; Roy, A. Chapter Renewable and Sustainable Materials in Automotive Industry. In *Encyclopedia of Renewable and Sustainable Materials*; Elsevier: Amsterdam, The Netherlands, 2019; pp. 162–179.
3. Hilditch, T.; Souza, T.; Hodgson, P. Chapter 2—Properties and automotive applications of advanced high-strength steels (AHSS). In *Welding and Joining of Advanced High Strength Steels (AHSS)*; Woodhead Publishing: Sawston, UK, 2015; pp. 9–28.
4. Santos, R.; Pereira, A.; Butuc, M.C.; Vincze, G.; Festas, A.; Moreira, L. Development of a Device Compatible with Universal Testing Machine to Perform Hole Expansion and Erichsen Cupping Tests. *Machines* **2019**, *8*, 2. [CrossRef]
5. *ISO 16630:2009*; Metallic Materials-Sheet and Strip-Hole Expanding Test. International Organization for Standardization: Geneva, Switzerland, 2009.
6. Hance, B. Practical Application of the Hole Expansion Test. *SAE Int. J. Engines* **2017**, *10*, 247–257. [CrossRef]
7. Yoon, J.I.; Jung, J.; Joo, S.H.; Song, T.J.; Chin, K.G.; Seo, M.H.; Kim, S.J.; Lee, S.; Kim, H.S. Correlation between fracture toughness and stretch-flangeability of advanced high strength steels. *Mater. Lett.* **2016**, *180*, 322–326. [CrossRef]
8. Dünckelmeyer, M.; Krempaszky, C.; Werner, E.; Doppler, C. Instrumented hole expansion test. *Mater. Sci.* **2009**, *8*, 50–57.
9. Panich, S.; Chongbunwatana, K. Influence of anisotropic yield criteria on simulation accuracy of the hole-expansion test. *IOP Conf. Ser. Mater. Sci. Eng.* **2020**, *967*, 012037. [CrossRef]
10. Leonhardt, A.; Kräusel, V.; Paar, U. Automated hole expansion test with pneumatic crack detection. *IOP Conf. Ser. Mater. Sci. Eng.* **2019**, *480*, 012026. [CrossRef]
11. Schreier, H.; Orteu, J.J.; Sutton, M.A. *Image Correlation for Shape, Motion and Deformation Measurements*; Springer US: New York, NY, USA, 2009. [CrossRef]
12. Behrens, B.A.; Diaz-Infante, D.; Altan, T.; Yilkiran, D.; Wölki, K.; Hübner, S. Improving Hole Expansion Ratio by Parameter Adjustment in Abrasive Water Jet Operations for DP800. *SAE Int. J. Mater. Manuf.* **2018**, *11*, 241–252. [CrossRef]
13. Chen, X.; Yang, L.; Chirac, C.; Du, C.; Zhou, D. *Measurement of Strain Distribution for Hole Expansion with Digital Image Correlation (DIC) System*; SAE: Warrendale, PA, USA , 2011. [CrossRef]
14. Li, J.; Wang, H.; Yan, D.W. Influence of Experiment Methods on Limit Hole Expansion Ratio. *DEStech Trans. Eng. Technol. Res.* **2016** . [CrossRef]
15. Krempaszky, C.; Larour, P.; Freudenthaler, J.; Werner, E. Towards More Efficient Hole Expansion Testing. In Proceedings of the IDDRG 2014 Conference, Paris, France, 1–4 June 2014 .
16. Wang, K.; Luo, M.; Wierzbicki, T. Experiments and modeling of edge fracture for an AHSS sheet. *Int. J. Fract.* **2014**, *187*, 245–268. [CrossRef]
17. Barlo, A.; Sigvant, M.; Pérez, L.; Islam, M.S.; Pilthammar, J. A Study of the Boundary Conditions in the ISO-16630 Hole Expansion Test. *IOP Conf. Ser. Mater. Sci. Eng.* **2022**, *1238*, 012031. [CrossRef]
18. Oh, S.H.; Yang, S.H.; Kim, Y.S. Chapter A study of image processing based hole expansion test. In *Testing and Measurement: Techniques and Applications*; CRC Press: London, UK, 2015; p. 8.
19. Pratt, W.K. *Digital Image Processing*; John Wiley & Sons, Inc.: Hoboken, NJ, USA, 2007. [CrossRef]
20. Gonzalez, R.C.; Woods, R.E. *Digital Image Processing*, 2nd ed.; Pearson: Upper Saddle River, NJ, USA, 2001.
21. Chiriac, C.; Chen, G. Formability Characterization of AHSS-Digital Camera Based Hole Expansion Test Development. In Proceedings of the International Deep Drawing Research Group IDDRG 2008 International Conference, Olofström, Sweden. 16–18 June 2008; pp. 16–18.
22. Kim, H.; Shang, J.; Beam, K.; Samant, A.; Hoschouer, C.; Dykeman, J. Development of new hole expansion testing method. *J. Phys. Conf. Ser.* **2016**, *734*, 032025. [CrossRef]
23. Choi, S.; Kim, K.; Lee, J.; Park, S.H.; Lee, H.J.; Yoon, J. Image Processing Algorithm for Real-Time Crack Inspection in Hole Expansion Test. *Int. J. Precis. Eng. Manuf.* **2019**, *20*, 1139–1148. [CrossRef]

24. Park, J.; Won, C.; Lee, H.J.; Yoon, J. Integrated Machine Vision System for Evaluating Hole Expansion Ratio of Advanced High-Strength Steels. *Materials* **2022**, *15*, 553. [CrossRef]

25. Cruz, D.J.; Santos, A.D.; Amaral, R.L.; Mendes, J.G.; Miranda, S.S.; Fernandes, J.V. Chapter An integrated methodology for HER determination in hole expansion test. In *Materials Design and Applications III*; Advanced Structured Materials; Springer International Publishing: Berlin/Heidelberg, Germany, 2021; pp. 243–256.

26. Duarte, J.F.; Santos, A.D.d.; da Rocha, A.B. Development of Testing Equipment for Sheet Metal Forming Analysis. In Proceedings of the IDDRG'94-International Deep Drawing Research Group 18th Biennial Congress, Conference Proceedings, Lisbon, Portugal, 16–20 May 1994; pp. 259–272.

27. Sousa, J. P. Desenvolvimento de um Sistema de Controlo e Aquisição de Dados para Máquina Universal de Ensaios de Chapas Metálicas. Master's Thesis, Faculdade de Engenharia da Universidade do Porto, Porto, Portugal, 2019.

28. Otsu, N. A Threshold Selection Method from Gray-Level Histograms. *IEEE Trans. Syst. Man Cybern.* **1979**, *9*, 62–66. [CrossRef]

29. Bradley, D.; Roth, G. Adaptive Thresholding using the Integral Image. *J. Graph. Tools* **2007**, *12*, 13–21. [CrossRef]

30. Soille, P. *Morphological Image Analysis*; Springer: Berlin/Heidelberg, Germany, 1999. [CrossRef]

31. Atherton, T.; Kerbyson, D. Size invariant circle detection. *Image Vis. Comput.* **1999**, *17*, 795–803. [CrossRef]

32. Yuen, H.; Princen, J.; Illingworth, J.; Kittler, J. Comparative study of Hough Transform methods for circle finding. *Image Vis. Comput.* **1990**, *8*, 71–77. [CrossRef]

33. Hough, P.V. Method and Means for Recognizing Complex Patterns. U.S. Patent 3,069,654, 18 December 1962

34. Duda, R.O.; Hart, P.E. Use of the Hough transformation to detect lines and curves in pictures. *Commun. ACM* **1972**, *15*, 11–15. [CrossRef]

35. Smereka, M.; Duleba, I. Circular Object Detection Using a Modified Hough Transform. *Appl. Math. Comput. Sci.* **2008**, *18*, 85–91. [CrossRef]

36. Canny, J. A Computational Approach to Edge Detection. *IEEE Trans. Pattern Anal. Mach. Intell.* **1986**, *PAMI-8*, 679–698. [CrossRef]

37. Parker, J.R. *Algorithms for Image Processing and Computer Vision*, 2nd ed.; John Wiley & Sons: Chichester, UK, 2010.

38. Marques, A.E.; Dib, M.A.; Khalfallah, A.; Soares, M.S.; Oliveira, M.C.; Fernandes, J.V.; Ribeiro, B.M.; Prates, P.A. Machine Learning for Predicting Fracture Strain in Sheet Metal Forming. *Metals* **2022**, *12*, 1799. [CrossRef]

39. *ISO 6892-1*; Metallic Materials-Tensile Testing-Method of Test at Room Temperature. International Organization for Standardization: Geneva, Switzerland, 2016.

40. Li, W.; Xia, M.; Peng, P.; Jia, Q.; Wan, Z.; Zhu, Y.; Guo, W. Microstructural evolution and deformation behavior of fiber laser welded QP980 steel joint. *Mater. Sci. Eng. A* **2018**, *717*, 124–133. [CrossRef]